# An Ultra-Low Noise Superconducting Antenna-Coupled Microbolometer With a Room-Temperature Read-Out

Arttu Luukanen, *Member, IEEE*, Erich N. Grossman, Aaron J. Miller, Panu Helistö, Jari S. Penttilä, Hannu Sipola, and Heikki Seppä

***Abstract*—In this letter, we report the electrical and optical characteristics of a superconducting vacuum-bridge microbolometer with an electrical noise equivalent power of 26 fW $\sqrt{\text{Hz}}$ and an effective time constant of 380 ns, when operated at a bath temperature of 4 K. We employ a novel room temperature external negative feedback readout architecture, that allows for noise matching to the device without bulky stepup transformers or cooled electronics. Both the detector and the readout lend themselves to be scaled to imaging arrays. The directly measured noise equivalent temperature difference over a 100–1000-GHz bandwidth is 125 mK in a 30-ms integration time.**

***Index Terms*—Bolometers, concealed weapons detection, superconducting detectors, THz detectors, THz imaging.**

## I. Introduction

IN RECENT years, the THz and submillimeter wave regions of the electromagnetic spectrum have been the subject of increasing attention due to the vast number of potential applications for chemical and biological stand-off detection, as well as the detection of concealed weapons and explosives hidden underneath clothing. The detection challenge is serious due to the limited availability of background-limited detectors, especially ones suited for construction of large imaging arrays. The figure of merit for passive radiometry of room temperature objects is the noise equivalent temperature difference (NETD), which corresponds to the minimum resolvable variation in the blackbody temperature over a specified post-detection integration time (typically 30 ms corresponding to video-rate imaging) and a specified optical throughput. For room temperature targets, the millimeter to THz frequencies lie within the Rayleigh–Jeans region of the spectrum.

## II. Description of the Bolometer

The microbolometers in this study are free-standing bridges of Nb atop $SiO_2$, approximately 1-$\mu$m-wide, suspended between the feedpoints of an equiangular spiral antenna patterned from an Al/Nb bilayer. The bolometers' basic electrical and thermal properties have been described elsewhere [1]. They differ significantly from conventional transition-edge bolometers [2], [3] in that large thermal gradients ($\sim$1 K/$\mu$m) are supported on the thermometer element during operation. This leads to a substantially different current-voltage characteristic, with major implications for readout architecture, as discussed below. The $I$–$V$ curve derives from the varying length of a normal metal "hotspot" [1], [4], located at the center of the thermally isolated bridge. Depending on the biasing conditions, an increase in the optical power tends to lengthen the "hotspot" which is responsible for generating all the voltage across the detector. A simple model based upon the one-dimensional (1-D) heat equation successfully predicts most properties of the detector. For a bridge with a critical temperature $T_c$ connected through a thermal conductance $G$ to the heat bath at $T_0$ the predicted $I$–$V$ curve has the form $I = V/R_n\{1+2[(p_o+p_e-1)+\sqrt{(p_o+p_e+1)^2-4p_o}]^{-1}\}$ where $R_n = R_{n0}(1+\alpha V^2/R_{n0}G)$ is the normal-state resistance which includes a small positive temperature coefficient of resistance $\alpha$ in the normal state, $p_o = P_{opt}/P_{sat}$ is the normalized optical power with $P_{opt}$ the incident THz power and $P_{sat} = G(T_c - T_{bath})$ the saturation power. The normalized electrical power is $p_e = V^2/(R_n P_{sat})$. In the limit $p_o \ll 1$ the expression for the $I$–$V$ reduces to the form in [1] $I = V/R_n + P_{sat}/V$.

Fabrication of the microbolometers differs only slightly from the process described in [1]. Briefly, a bilayer of 50-nm-thick Nb and 100-nm-thick Al is deposited atop a thermally oxidized (oxide thickness is 50 nm), high resistivity Si wafer. The nominal bridge dimensions are $1 \times 36\ \mu m^2$. The release of the Nb strip to a free-standing bridge was achieved by opening two windows to the $SiO_2$ adjacent to the bridge, and performing a $XeF_2$ gas-phase chemical etch of the underlying Si. The etching of the Nb was prevented by the $SiO_2$ from below and a protective photoresist from the top. Finally, after the dicing of the wafer, the photoresist was removed in an $O_2$ plasma ash.

## III. Measurement Setup

The devices are mounted metal layers up against a 4-mm diameter, high resistivity Si hyperhemisphere, held in place below the device chip with mechanical pressure from an Al flexure mount. The normal-state resistance of the 36:1 aspect ratio device was $\sim$60 $\Omega$. In the experiments, a novel readout scheme [5] is employed that exploits the modest curvature in the $I$–$V$ curve

Manuscript received January 15, 2006.

A. Luukanen is with the National Institute of Standards and Technology, Boulder, CO 80305 USA and also with the MilliLab, VTT Technical Research Centre of Finland, Espoo FIN-02044, Finland (e-mail: arttu.luukanen@vtt.fi).

E. N. Grossman is with the National Institute of Standards and Technology, Boulder, CO 80305 USA.

A. J. Miller is with the National Institute of Standards and Technology, Boulder, CO 80305 USA and also with Albion College, Albion, MI, 49224 USA.

P. Helistö, J. S. Penttilä, H. Sipola, and H. Seppä are with VTT Technical Research Centre of Finland, Espoo FIN-02044, Finland.

Digital Object Identifier 10.1109/LMWC.2006.879483

1531-1309/$20.00 © 2006 IEEE

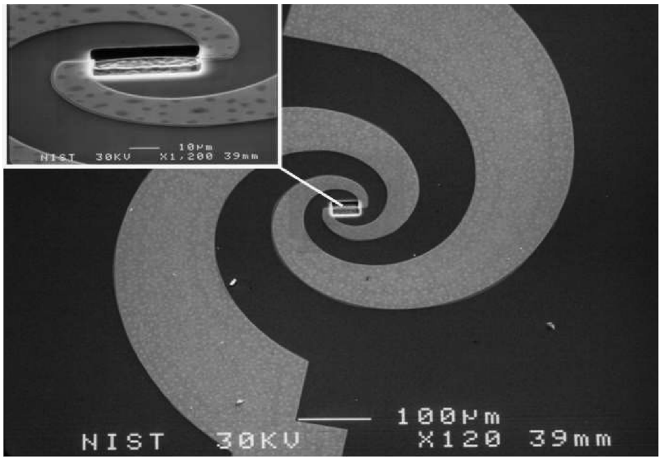


Fig. 1. SEM micrograph of the detector. The inset shows in detail the suspended 36 $\mu$m $\times$ 1 $\mu$m $\times$ 50-nm bridge.

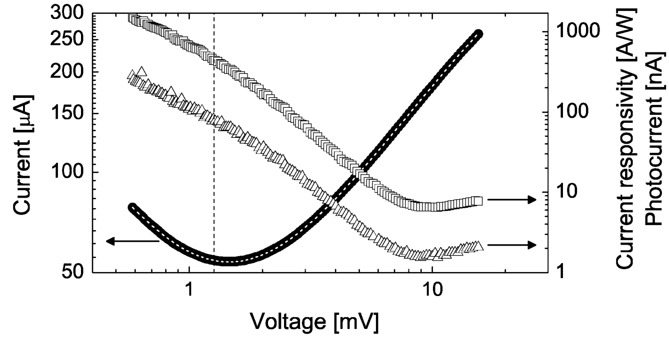


Fig. 2. $I$–$V$ curve of the bolometer (circles) with the current shown on the left vertical axis. The dashed line indicates the fit to the theory, yielding $G =$ 14 nW/K and $R_{\rm n} = 54\ \Omega$. The right vertical axis corresponds to the electrical responsivity derived from the measured $I$–$V$ curve of the detector, $\mathcal{R}_{\rm I} = -V^{-1}\mathcal{L}/(1+\mathcal{L})$, as a function of bias voltage, represented by the rectangles. The measured peak-to-peak signal current from a chopped 77-K blackbody is represented by the triangles (in nA), and shows that the voltage dependencies of the optical and electrical responsivities agree. The dashed vertical line represents the optimum operating point of 1.26 mV.

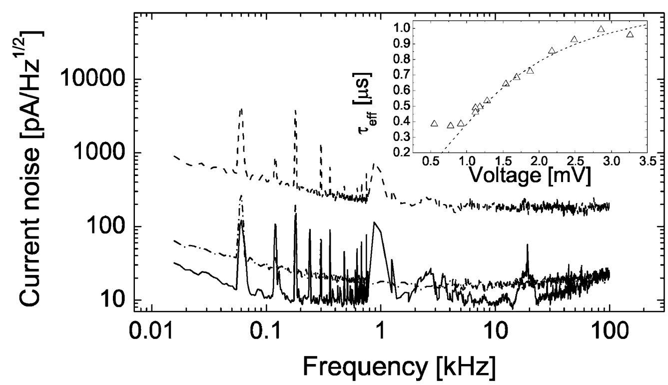


Fig. 3. Three noise spectra from the device at different bias points. The solid line, representing lowest NEP, was acquired at $V = 1.26$ mV, corresponding to the optimum operating point. The dashed and dash-dotted lines represent spectra acquired at $V = 0.56$ mV and $V = 16$ mV, respectively. The features at 60-Hz multiples are due to electromagnetic pickup in the detector cabling, and can be removed with better shielding. The inset shows the dependence of the effective time constant of the bolometer on the bias voltage. Best fit yields an intrinsic time constant $\tau_0 = 1.2\ \mu$s. The minimum value for $\tau_{\rm eff} = 380$ ns. Below this value the response time is limited by the bandwidth of our readout electronics.

of a hotspot microbolometer. Near the minimum current in the $I$–$V$ curve, the bolometer's dynamic impedance $dV/dI \gg R_{\rm n}$, which implies that the voltage noise from a conventional room-temperature bipolar amplifier can be much less than the detector's own Johnson noise. The modest curvature in the $I$–$V$ implies that this detector-limited noise condition can be obtained over a practical range of bias voltage. This would not be true in a conventional voltage biased TES bolometer, where the isothermal thermometer generates a sharp "kink" in the $I$–$V$ at the minimum current (see Fig. 1).

## IV. Electrical Characteristics of the Bolometer

The critical temperature of the bolometer was obtained using an ac four-wire measurement with the device in the dark. For the critical temperature we obtained a $T_{\rm c} = 7$ K, which is below the nominal value of 9 K for Nb, but close to what was measured on evaporated Nb devices described in [1]. A measured $I$–$V$ curve for a typical $1 \times 36\ \mu{\rm m}^2$ bolometer is shown in Fig. 2, along with a least-squares fit to the theoretical expression using $R_{\rm n0}$, $\alpha$ and $G$ as fitting parameters in the limit $p_{\rm o} \ll 1$. Agreement is very good. The measured photocurrent and best-fit model of the electrical responsivity, i.e., $dI/dP_{\rm opt}|_{V={\rm const}}$ is displayed on the same voltage scale. The photocurrent measurement was performed by placing a polyethylene lens just outside the cryostat window and an optical chopper whose blades were covered with room temperature ($\sim$295 K) mm-wave absorber material at the resulting focus of the lens. A 77-K absorber, large enough to fill the chopper blade's aperture was then placed just beyond the chopper wheel. The synchronously detected current signal is then proportional to the optical responsivity.

The time constant is measured directly from the photocurrent response to a 100-ns pulse of 95-GHz radiation from a pulsed IMPATT oscillator, and the fitted time constant of a single exponential decay is displayed in the inset to Fig. 3, along with noise spectra measured as several bias points along the $I$–$V$ curve. The effective time constant of the device is reduced according to the electrothermal feedback with $\tau_{\rm eff} = \tau_0/(1+\mathcal{L})$ [8] where $\mathcal{L} = R_n G \Delta T/V^2$ is the electrothermal loop gain [1]. Best fit yields $\tau_0 = 1.2\ \mu$s. At the optimum bias point of $V = 1.26$ mV, about 0.13 mV below the minimum in the $I$–$V$ curve and at 78 Hz (the chopping frequency), the noise spectral density is 11.7 pA/$\sqrt{\rm Hz}$. The spikes in the spectra are due to EMI, picked up by the wiring and detected by the bolometer. This can be reduced significantly with improved shielding. As expected, the noise spectral density at all frequencies rises sharply as the bias point is moved above or below the voltage of the current minimum, reflecting rapidly increasing contributions from the uncooled amplifier. From the $I$–$V$ curve, an electrical responsivity of $-$ 445 A/W and an electrical noise equivalent power (NEP$_{\rm e}$) of 26 fW/$\sqrt{\rm Hz}$ is obtained (see Fig. 4).

## V. Optical Characterization

The absolute values of optical responsivity and optical NEP require an accurate estimate of the power incident on the device. The optical path intercepts two fluorogold low-pass filters (cut-off at 1 THz): a 3-mm-thick filter at 4 K, and a 1-mm-thick one at 77 K. Optical access to the dewar is through a teflon vacuum window. The nominal bandwidth coupled to

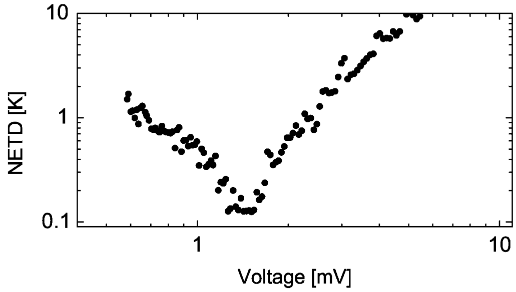


Fig. 4. Measurement of the NETD using a chopped blackbody yields NETD= 125 mK at an integration time of 30 ms.

TABLE I
BOLOMETER PARAMETERS [6], [7]

| **Bolometer properties** | | |
|---|---|---|
| $R_{n0}$ | 54 Ω | |
| $\alpha$ | $0.4 \cdot 10^{-3}$ K$^{-1}$ | |
| $G$ | 14 nW/K | |
| $\tau_0$ | 1.2 $\mu$s | |
| $\tau_{\mathrm{eff}}$ at V=1.26 mV | 520 ns | |
| $\tau_{\mathrm{eff}}$ min. | 380 ns | |
| **Optical parameters (0.1 to 1 THz)** | Calculated | Measured |
| Teflon window transmission [6] | 94 % | |
| 77 K Fluorogold transmission [6] | 56 % | |
| 4 K Fluorogold transmission [6] | 73 % | |
| Si lens transmission | 70 % | |
| Antenna-bolometer coupling at $V$ = 1.26 mV | 34 % | |
| Total efficiency referred to the window | 9 % | 7 % |
| Total efficiency referred to the detector | 24 % | 18 % [7] |

the antenna designed for 75–1200 GHz is limited at the high frequency end by the 1-THz cutoff of the Fluorogold filters. Thus, the optical blackbody power incident in single mode at the dewar window is $k_{\mathrm{B}}(295\ \mathrm{K} - 77\ \mathrm{K})\Delta f \approx 2.7$ nW. The estimated efficiencies for the optical components are summarized in Table I. The antenna-bolometer interface transmits 30% of the power due to an impedance mismatch between the 75-Ω log-spiral impedance and the $(25 + 137i)\ \Omega$ bolometer. The reactive part is due to a geometric inductance of 34 pH calculated for our geometry using (8) in [9]. The expected overall system optical efficiency of 7% referred to the input of the dewar agrees well with the measurement, which yielded 9% at the optimum bias point. The corresponding system optical $\mathrm{NEP}_{\mathrm{opt}} = 0.4$ pW/$\sqrt{\mathrm{Hz}}$. Significant improvement in coupling is possible by the use of thinner Fluorogold filters, and by increasing the normal state resistance of the device which improves the coupling efficiency and reduces $\mathrm{NEP}_{\mathrm{e}}$. With these improvements only, we estimate that a system optical efficiency of 20% and a system optical $\mathrm{NEP}_{\mathrm{opt}}$ <25 fW/$\sqrt{\mathrm{Hz}}$ can be achieved. In fact, in our previous work a similar device architecture with a normal state resistance of 120 Ω demonstrated a $\mathrm{NEP}_{\mathrm{e}}$ of 14 fW/$\sqrt{\mathrm{Hz}}$ [1]. NETD can be measured directly, without requiring any estimate of bandwidth or efficiency, simply by comparing the noise in the measured photocurrent with the photocurrent signal from a source of known temperature difference—the 77–295 K blackbody in our case. This yields $S_{\mathrm{T}}^{1/2} = 31$ mK/$\sqrt{\mathrm{Hz}}$, or $\mathrm{NETD} = S_{\mathrm{T}}^{1/2}/\sqrt{2\tau} = 125$ mK in a 30-ms time constant. In addition to the electrical and optical characterization reported here, we have recorded passive THz images on a number of subjects relevant to indoor CWD applications, which will be described in a separate publication.

## VI. CONCLUSION

In summary, we have described the optical performance of a free-standing Nb microbolometer, coupled to a broadband spiral antenna covering 0.1–1.2 THz. Its fabrication and novel readout scheme are amenable to incorporation in large focal-plane arrays. Its performance, described by NETD $=$ 125 mK, $\mathrm{NEP}_e = 26$ fW/$\sqrt{\mathrm{Hz}}$, $\mathrm{NEP}_{\mathrm{opt}} = 0.4$ pW/$\sqrt{\mathrm{Hz}}$ and $\tau_{\mathrm{eff}} = 380$ ns, is a major improvement over any existing uncooled detector technology. With an increase of the bolometer resistance and by reducing the optical loss in the filters we are confident that a NETD approaching the ≈4 mK photon-noise limit and a $\mathrm{NEP}_{\mathrm{opt}}$ <25 fW/$\sqrt{\mathrm{Hz}}$ can be achieved. Once this level of sensitivity is reached, our plan is to implement the use of an already constructed circular variable filter based on a frequency-selective surface to enable low-resolution imaging spectrometry for materials identification. Advances in closed-cycle cryocooler technology over the last several years [10] may make the cost-performance tradeoff favorable to the hotspot microbolometers described here in many concealed-weapons detection applications.

## ACKNOWLEDGMENT

The authors wish to thank M. Kiviranta for useful discussions and assistance with the transimpedance readout.

## REFERENCES

[1] A. Luukanen and J. P. Pekola, "A superconducting antenna-coupled hot-spot microbolometer," *Appl. Phys. Lett.*, vol. 82, pp. 3970–3972, Jun. 2003.
[2] K. D. Irwin, G. C. Hilton, D. A. Wollman, and J. M. Martinis, "X-ray detection using a superconducting transition-edge sensor microcalorimeter with electrothermal feedback," *Appl. Phys. Lett.*, vol. 69, no. 13, pp. 1945–1947, Sep. 1996.
[3] A. T. Lee, P. L. Richards, S. W. Nam, B. Cabrera, and K. D. Irwin, "A superconducting bolometer with strong elecrothermal feedback," *Appl. Phys. Lett.*, vol. 69, no. 12, pp. 1801–1803, Sep. 1996.
[4] D. W. Floet, E. Miedema, and T. Klapwijk, "Hotspot mixing: A framework for heterodyne mixing in superconducting hot-electron bolometers," *Appl. Phys. Lett.*, vol. 74, no. 3, pp. 433–435, 1999.
[5] J. Penttilä, H. Sipola, P. Helistö, and H. Seppä, "Low Noise Readout of Superconducting Bolometers Based on Electrothermal Feedback," *Supercond. Sci. Technol.*, pp. 319–322, Nov. 2006.
[6] M. Halpern, H. P. Gush, E. Wishnow, and V. De Cosmo, "Far infrared transmission of dielectrics at cryogenic and room temperatures: glass, fluorogold, eccosorb, stycast, and various plastics," *Appl. Opt.*, vol. 25, no. 4, pp. 565–570, 1986.
[7] Obtained using the calculated values for the other components.
[8] K. D. Irwin, G. C. Hilton, D. A. Wollman, and J. M. Martinis, "Thermal-response time of superconducting transition-edge microcalorimeters," *J. Appl. Phys.*, vol. 83, no. 8, pp. 3978–3985, 1998.
[9] D. Jaisson, "Planar impedance transformer," *IEEE Trans. Microw. Theory Tech.*, vol. 47, no. 5, pp. 592–595, May 1999.
[10] H. J. M. ter Brake and G. F. M. Wiegerinck, "Low-power cryocooler survey," *Cryogenics*, vol. 42, no. 11, pp. 705–718, 2002.